

A Spatially Distributed Multi-Period Optimal Power Flow Study with Distributed Battery Units

Aryan Ritwajeet Jha*, *SIEEE*, Subho Paul†, *MIEEE*, Anamika Dubey*, *SMIEEE*

**School of Electrical Engineering & Computer Science, Washington State University, Pullman, WA, USA*

†*Department of Electrical Engineering, Indian Institute of Technology (BHU) Varanasi, Varanasi, UP, India*

*{aryan.jha, anamika.dubey}@wsu.edu, †{subho.eee}@iitbhu.ac.in

Abstract—The growing presence of battery-associated distributed energy resources in distribution networks necessitates the development of multi-period optimal power flow (MPOPF). Generally, the MPOPF frameworks are developed as mixed integer non-convex programming (MINCP) and solved centrally. However, the main limitation of centralized MPOPF (MPCOPF) is its longer solution time, a typical solution time is in the order of 10^3 to 10^4 seconds. To overcome such deficiencies, this article proposes a spatially distributed MPOPF (MPDOPF)

Index Terms—Batteries, distribution network, distributed energy resources (DERs), equivalent network approximation (ENApp)

I. INTRODUCTION

Presently, optimal power flow (OPF) tools are developed to run the MV/LV distribution grids in the most economical, reliable, and secure manner. The usefulness of OPF studies is gaining more interest due to the penetration of distributed energy resources (DERs), especially solar photovoltaic panels. Power generation from these DERs is influenced by the weather conditions, hence highly intermittent. Presently, deployment of battery units is becoming more pertinent to mitigate the uncertainty effect and maintain the power balance by controlling the charging and/or discharging operations [1]. However, the inclusion of batteries converts the conventional single-period time-decoupled OPF problem into a multi-period time-coupled OPF analysis.

Traditionally, centralized OPF (COPF) methods were popular where grid-edge data are accumulated at a central controller location [2]. The central controller is responsible for processing the accumulated data, solving the OPF algorithm, and dispatching control signals to the controlling resources. The centralized OPF algorithms are generally developed as a mixed integer non-convex programming (MINCP) problem and then simplified either as a convex problem by adopting second-order cone programming (SOCP) relaxations [3] [4], or as a linear problem by adopting Taylor series expansion [2], polyhedral approximations [5] or linear power flow models [6].

To overcome the scalability issues related to the COPF methods, distributed OPF (DOPF) algorithms are often proposed by decomposing the original COPF problem into multiple sub-problems, solved in parallel by permitting neighborhood communication. In this regard, the Auxiliary Problem Principle (APP) and the Alternating direction method of multipliers (ADMM) are two popular algorithms that are

used to solve OPF problems as quadratic convex [7], SOCP relaxed convex [8], semidefinite programming (SDP) relaxed convex [9], [10], and linear programming problems [11]. Previously in [12], the authors' research group developed a DOPF framework based on the Equivalent Network Approximation method (ENApp) for solving DOPF problems with lesser macro iterations compared to ADMM.

The above references [3]- [11] mainly focused on developing single-time step OPF problems by neglecting the grid-edge devices having time-coupled operation, like batteries. The inclusion of battery models transforms a single-time step OPF into a multi-period OPF (MPOPF). Reference [13] propound a nonlinear multi-period centralized OPF (MPCOPF) framework to solve the active-reactive power dispatch from the batteries and DERs in a distribution network. Wu et al. [14] framed an MPCOPF problem for a virtual power plant (VPP) collocated distribution network. The original centralized multi-parametric quadratic problem is decomposed into one master and multiple sub-problems for distribution network and VPPs, respectively by utilizing the concept of Benders Decomposition (BD). However, BD suffers from slow convergence. Alizadeh and Capitanescu [15] proposed a stochastic security-constrained MPCOPF which is solved by sequentially solving a specific number of linear approximations of the original problem. Usman and Capitanescu [16] developed three different MPCOPF frameworks to solve stochastic AC OPF problems. All three approaches start by solving a linear program to fix the binary variables followed by either a linear or non-linear program to determine the continuous variables.

It is evident from the above

A taxonomy table to compare the existing studies and the present work is provided in I.

The specific contributions are as follows:

- 1) The overall problem is formulated as a non-convex programming and the

II. PROBLEM FORMULATION

A. Notations

In this study, the distribution network is accounted as a tree (connected graph) having N number of buses (indexed with i , j , and k) and the study is conducted for T time steps (indexed by t), each of interval length Δt . The distribution line connecting two buses i and j are denoted by ij (having

TABLE I: TAXONOMY TABLE FOR COMPARISON

References	DERs	Batteries	Single period OPF	Multi-period OPF	Centralized OPF	Distributed OPF	Framework
[6]			✓		✓		Linear
[3]			✓		✓		Convex
[5]	✓		✓		✓		Linear
[1]- [4]	✓			✓			✓
[1], [4]		✓		✓			✓
[7]	✓		✓			✓	Convex (APP)
[8]- [10]	✓		✓			✓	Convex (ADMM)
[13]	✓	✓		✓	✓		Non-convex
This paper	✓	✓		✓		✓	Non-convex (ENApp)

resistance and reactance of r_{ij} ohm and x_{ij} ohm, respectively) and magnitude of the current flowing through the line at time t is denoted by I_{ij}^t ($l_{ij}^t = (I_{ij}^t)^2$). The voltage magnitude of bus i at time t is given by $V_i^t \in [V_{min}, V_{max}]$ ($v_i^t = (V_i^t)^2$). Apparent power demand at a node j at time t is $s_{Lj}^t (= p_{Lj}^t + jq_{Lj}^t)$. The uncontrolled active power generation from the DER present at bus j at time step t is denoted by p_{Dj}^t and controlled reactive power dispatch from the DER inverter is q_{Dj}^t . Static capacitance attached to a node j is denoted by q_{Cj} . The apparent power flow through line ij at time step t is $S_{ij}^t (= P_{ij}^t + jQ_{ij}^t)$. The battery state of charge (soc) or energy level is B_j^t . Charging and discharging active power from battery inverter (of apparent power capacity $S_{R,j}^t$) are denoted by P_{cj}^t and P_{dj}^t , respectively. The total state of charge capacity of the batteries are denoted by $E_{R,j}$, and the Rated battery powers are denoted by $P_{B_{R,j}}$. The reactive power support of the battery inverter is q_{Bj}^t . Rated apparent powers of DERs and Batteries at node j are denoted by $S_{D_{R,j}}$ and $S_{B_{R,j}}$ respectively.

B. Centralized Multi-Period OPF with Batteries

The OPF problem given in (1) aims to minimize the cost of power borrowed from the substation for the entire horizon. The incorporation of an additional 'Battery Loss' term helps us bypass using binary (integer) constraints for modelling the operation of batteries, which would otherwise make the optimization problem harder to solve. The term still ensures the complementarity of charging and discharging operations for any battery during a particular time period [17]–[19].

$$\min \sum_{t=1}^T \left[C^t P_{Subs}^t + \alpha \sum_{j \in \mathcal{B}} \left\{ (1 - \eta_C) P_{Cj}^t + \left(\frac{1}{\eta_D} - 1 \right) P_{Dj}^t \right\} \right] \quad (1)$$

Subject to the constraints (2) to (13) given below:

$$0 = \sum_{(j,k) \in \mathcal{L}} \{P_{jk}^t\} - (P_{ij}^t - r_{ij} l_{ij}^t) - (P_{dj}^t - P_{cj}^t) - p_{Dj}^t + p_{Lj}^t \quad (2)$$

$$0 = \sum_{(j,k) \in \mathcal{L}} \{Q_{jk}^t\} - (Q_{ij}^t - x_{ij} l_{ij}^t) - q_{Dj}^t - q_{Bj}^t + q_{Lj}^t \quad (3)$$

$$0 = v_i^t - v_j^t - 2(r_{ij} P_{ij}^t + x_{ij} Q_{ij}^t) + \{r_{ij}^2 + x_{ij}^2\} l_{ij}^t \quad (4)$$

$$0 = (P_{ij}^t)^2 + (Q_{ij}^t)^2 - l_{ij}^t v_i^t \quad (5)$$

$$P_{Subs}^t \geq 0 \quad (6)$$

$$l_{ij}^t \in [0, I_{R,ij}^2] \quad (7)$$

$$v_j^t \in [V_{min}^2, V_{max}^2] \quad (8)$$

$$q_{Dj}^t \in \left[-\sqrt{S_{D_{R,j}}^2 - p_{Dj}^t{}^2}, \sqrt{S_{D_{R,j}}^2 - p_{Dj}^t{}^2} \right] \quad (9)$$

$$0 = B_j^t - \left\{ B_j^{t-1} + \Delta t \eta_c P_{cj}^t - \Delta t \frac{1}{\eta_d} P_{dj}^t \right\} \quad (10)$$

$$P_{cj}^t, P_{dj}^t \in [0, P_{B_{R,j}}] \quad (11)$$

$$q_{Bj}^t \in [-0.44 P_{B_{R,j}}, 0.44 P_{B_{R,j}}] \quad (12)$$

$$B_j^t \in [soc_{min} B_{R,j}, soc_{max} B_{R,j}] \quad (13)$$

The distribution network is represented with the help of the branch power flow equations (2) to (5). Constraints (2) and (3) signify the active and reactive power balance at node j . The KVL equation for branch (i, j) is represented by (4), while the equation describing the relationship between current magnitude, voltage magnitude and apparent power magnitude for nodes i and j is (5). Backflow of real power into the substation from the distribution system is avoided using the constraint (6). The box limits for squared branch current and squared node voltage are enforced via (7) and (8). (9) describes the reactive power limits of DER inverters. The trajectory of the state of charge of batteries versus time is given by (10) and is the only class of constraints in this paper coupling the optimal power flow problem in time. Battery charging and discharging powers are non-negative valued variables which should not exceed the battery's rated power capacity, as given by (11). Every battery's reactive power is also constrained based on the associated inverter's rated capacity, as described by (12). For safe and sustainable operation of the batteries, the state of charge B_j^t is constrained to be within some percentage limits of the rated battery soc capacity, as given in (13).

C. ENApp based Distributed Multi-Period OPF with Batteries

III. CASE STUDY DEMONSTRATION

A. Simulation Data: IEEE 123 Bus Test System

We're using a Balanced Three-Phase version of the IEEE 123 Bus Test System, which has 85 Load Nodes. Additionally, 20% (17) and 30% (26) of these load nodes also contain reactive power controllable Solar photovoltaics (PVs) and Batteries respectively. Their ratings are as per Table II. To

demonstrate the effectiveness of the proposed algorithm, the Test System has been divided into four areas on similar lines as [12]. The full test system along with the area-wise division is shown in Figure 1.

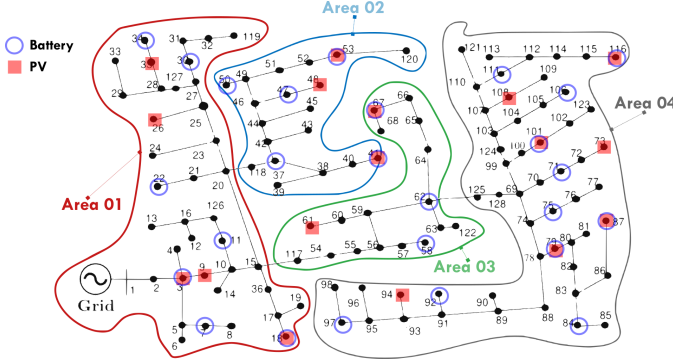


Fig. 1: IEEE 123 Node System Divided Into Four Areas

To showcase the workflow of the proposed algorithm, simulations were run for a 5 time-period horizon. Figure 2 shows the forecasted profiles for load, solar irradiance and cost of substation power over the horizon.

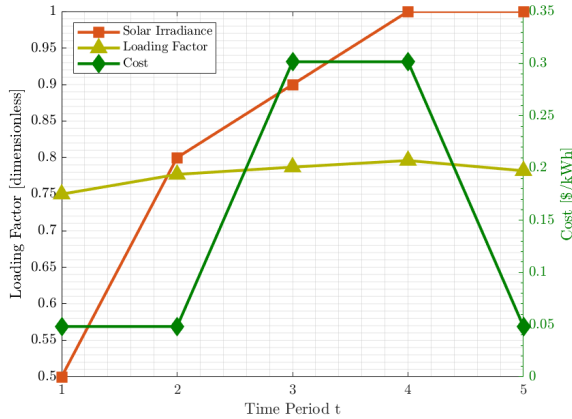


Fig. 2: Forecasts for Demand Power, Irradiance and Cost of Substation Power over a 5 Hour Horizon

TABLE II: Parameter Values

Parameter	Value
V_{min}, V_{max}	0.95, 1.05
p_{DR_j}	$0.33p_{LR_j}$
s_{DR_j}	$1.2p_{DR_j}$
P_{BR_j}	$0.33p_{LR_j}$
B_{R_j}	$T_{fullCharge} \times P_{BR_j}$
$T_{fullCharge}$	4 h
Δt	1 h
η_C, η_D	0.95, 0.95
soc_{min}, soc_{max}	0.30, 0.95
α	0.001

B. Simulation Workflow

We use MATLAB 2023a to set up our simulations. This includes both the high level algorithms as well as calling the optimization solver. We use MATLAB's `fmincon` function to parse nonlinear nonconvex optimization problem described by (1) to (13) and the SQP optimization algorithm to solve it. Once the simulations are completed and resulting optimal control variables obtained, they are passed through an OpenDSS engine (which already has the known system data and forecasted values configured) in order to check for the feasibility of the results. The associated code may be found here.

C. Simulation Results

The Test System

1) *Comparison between MPCOPF and MPDOPF*: In this section, comparative analyses are carried out between MPCOPF and MPDOPF considering 5-hour time steps.

TABLE III: Comparative analyses between MPCOPF and MPDOPF - 5 time-period horizon

Metric	MPCOPF	MPDOPF
Biggest subproblem size		
Decision variables	3150	1320
Linear constraints	5831	2451
Nonlinear constraints	635	265
Simulation results		
Substation power cost (\$)	576.31	576.30
Substation real power (kW)	4308.28	4308.14
Line loss (kW)	75.99	76.12
Substation reactive power (kVAR)	574.18	656.24
PV reactive power (kVAR)	116.92	160.64
Battery reactive power (kVAR)	202.73	76.01
Computation		
Number of Iterations	-	5
Total Simulation Time (s)	521.25	49.87

Further, here the

TABLE IV: ACOPF feasibility analyses - 5 time-period horizon

Metric	MPDOPF	OpenDSS
Full horizon		
Substation real power (kW)	4308.14	4308.35
Line loss (kW)	76.12	76.09
Substation reactive power (kVAR)	656.24	652.49
Max. all-time discrepancy		
Voltage (pu)		0.0002
Line loss (kW)		0.0139
Substation power (kW)		0.3431

Boundary Variable Plots are too tall, make them slightly shorter, like 25% of the page only.

D. Scalability Analysis

To demonstrate the effectiveness of the proposed algorithm over a bigger horizon to demonstrate scalability, simulations were run for a 10 time-period horizon. Figure 6 shows the forecasted profiles for load, solar irradiance and cost of substation power over the horizon.

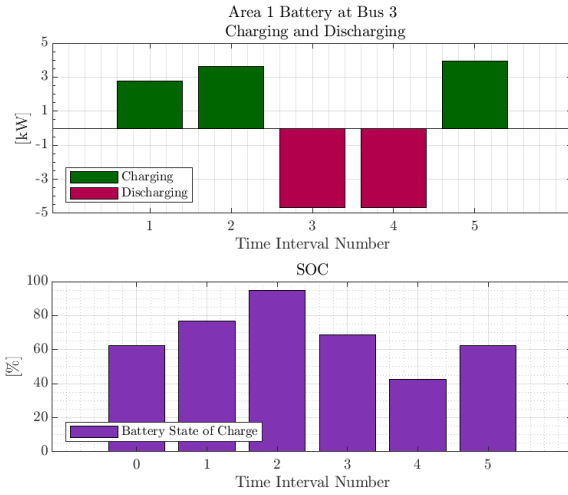


Fig. 3: Charging-Discharging and SOC graphs for Battery at Bus 3 located in Area 1 obtained by MPDOPF

1) *Comparison between MPCOPF and MPDOPF*: In this section, comparative analyses are carried out between MPCOPF and MPDOPF considering 10-hour time steps with 20% PV penetration and 30% battery penetration.

TABLE V: Comparative analyses between MPCOPF and MPDOPF - 10 time-period horizon

Metric	MPCOPF	MPDOPF
Biggest subproblem size		
Decision variables	6300	2640
Linear constraints	11636	4891
Nonlinear constraints	1270	530
Simulation results		
Substation power cost (\$)	1197.87	1197.87
Substation real power (kW)	8544.28	8544.04
Line loss (kW)	148.67	148.94
Substation reactive power (kVAR)	1092.39	1252.03
PV reactive power (kVAR)	222.59	139.81
Battery reactive power (kVAR)	388.52	310.94
Computation		
Number of Iterations	-	5
Total Simulation Time (s)	4620.73	358.69

Further, here the

TABLE VI: ACOPF feasibility analyses - 10 time-period horizon

Metric	MPDOPF	OpenDSS
Full horizon		
Substation real power (kW)	8544.04	8544.40
Line loss (kW)	148.94	148.87
Substation reactive power (kVAR)	1252.03	1243.36
Max. all-time discrepancy		
Voltage (pu)	0.0002	
Line loss (kW)	0.0132	
Substation power (kW)	0.4002	

Lorem ipsum dolor sit amet, consectetur adipiscing elit. Ut purus elit, vestibulum ut, placerat ac, adipiscing vitae, felis. Curabitur dictum gravida mauris. Nam arcu libero, nonummy eget, consectetur id, vulputate a, magna. Donec vehicula

augue eu neque. Pellentesque habitant morbi tristique senectus et netus et malesuada fames ac turpis egestas. Mauris ut leo. Cras viverra metus rhoncus sem. Nulla et lectus vestibulum urna fringilla ultrices. Phasellus eu tellus sit amet tortor gravida placerat. Integer sapien est, iaculis in, pretium quis, viverra ac, nunc. Praesent eget sem vel leo ultrices bibendum. Aenean faucibus. Morbi dolor nulla, malesuada eu, pulvinar at, mollis ac, nulla. Curabitur auctor semper nulla. Donec varius orci eget risus. Duis nibh mi, congue eu, accumsan eleifend, sagittis quis, diam. Duis eget orci sit amet orci dignissim rutrum.

IV. CONCLUSIONS

[17], [18], [20]–[22]

REFERENCES

- [1] T. Gangwar, N. P. Padhy, and P. Jena, "Storage allocation in active distribution networks considering life cycle and uncertainty," *IEEE Trans. Ind. Inform.*, vol. 19, no. 1, pp. 339–350, Jan. 2023.
- [2] S. Paul and N. P. Padhy, "Real-time advanced energy-efficient management of an active radial distribution network," *IEEE Syst. J.*, vol. 16, no. 3, pp. 3602–3612, Sept. 2022.
- [3] W. Wei, J. Wang, and L. Wu, "Distribution optimal power flow with real-time price elasticity," *IEEE Trans. Power Syst.*, vol. 33, no. 1, pp. 1097–1098, Jan. 2018.
- [4] M. M.-U.-T. Chowdhury, B. D. Biswas, and S. Kamalasadan, "Second-order cone programming (sopc) model for three phase optimal power flow (opf) in active distribution networks," *IEEE Trans. Smart Grid*, vol. 14, no. 5, pp. 3732–3743, 2023.
- [5] Z. Guo, W. Wei, L. Chen, Z. Dong, and S. Mei, "Parametric distribution optimal power flow with variable renewable generation," *IEEE Trans. Power Syst.*, vol. 37, no. 3, pp. 1831–1841, May 2022.
- [6] H. Yuan, F. Li, Y. Wei, and J. Zhu, "Novel linearized power flow and linearized opf models for active distribution networks with application in distribution lmp," *IEEE Trans. Smart Grid*, vol. 9, no. 1, pp. 438–448, Jan. 2018.
- [7] A. R. Di Fazio, C. Risi, M. Russo, and M. De Santis, "Decentralized voltage optimization based on the auxiliary problem principle in distribution networks with ders," *Appl. Sci.*, vol. 11, no. 4509, pp. 1–24, 2021.
- [8] W. Zheng, W. Wu, B. Zhang, H. Sun, and Y. Liu, "A fully distributed reactive power optimization and control method for active distribution networks," *IEEE Trans. Smart Grid*, vol. 7, no. 2, pp. 1021–1033, Mar. 2016.
- [9] P. Wang, Q. Wu, S. Huang, C. Li, and B. Zhou, "Admm-based distributed active and reactive power control for regional ac power grid with wind farms," *J. Modern Power Syst. Clean Energy*, vol. 10, no. 3, pp. 588–596, May 2022.
- [10] B. D. Biswas, M. S. Hasan, and S. Kamalasadan, "Decentralized distributed convex optimal power flow model for power distribution system based on alternating direction method of multipliers," *IEEE Trans. Ind. Appl.*, vol. 59, no. 1, pp. 627–640, Jan.-Feb. 2023.
- [11] S. Paul, B. Ganguly, and S. Chatterjee, "Nesterov-type accelerated admm (n-admm) with adaptive penalty for three-phase distributed opf under non-ideal data transfer scenarios," in *2023 IEEE 3rd International Conference on Smart Technologies for Power, Energy and Control (STPEC)*, 2023, pp. 1–6.
- [12] R. Sadnan and A. Dubey, "Distributed optimization using reduced network equivalents for radial power distribution systems," *IEEE Trans. Power Syst.*, vol. 36, no. 4, pp. 3645–3656, Jul. 2021.
- [13] A. Gabash and P. Li, "Active-reactive optimal power flow in distribution networks with embedded generation and battery storage," *IEEE Trans. Power Syst.*, vol. 27, no. 4, pp. 2026–2035, Nov. 2012.
- [14] C. Wu, W. Gu, S. Zhou, and X. Chen, "Coordinated optimal power flow for integrated active distribution network and virtual power plants using decentralized algorithm," *IEEE Trans. Power Syst.*, vol. 36, no. 4, pp. 3541–3551, Jul. 2021.

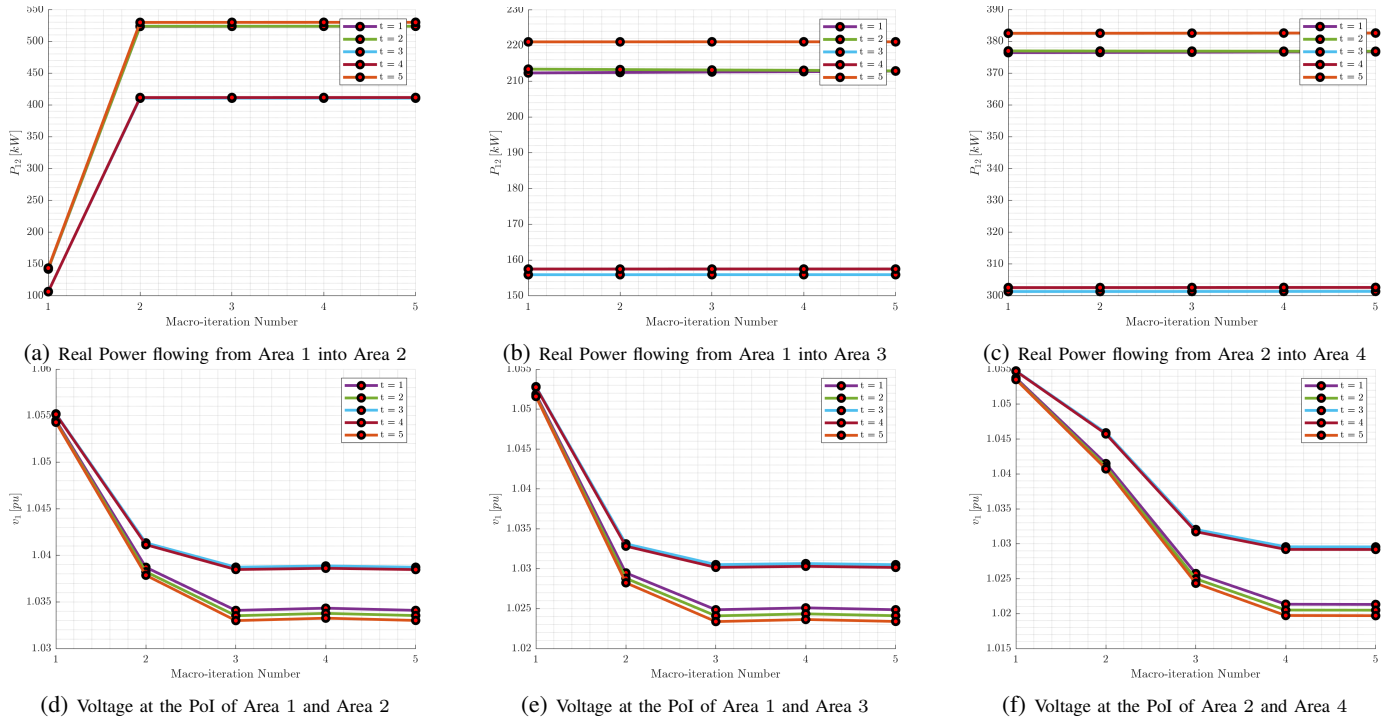


Fig. 4: Convergence of Boundary variables with every iteration. Each plot represents a particular variable exchanged between a pair of connected areas. Each line graph within a plot represents a particular time period.



Fig. 5: Convergence of Objective Function Value with each MPDOPF iteration

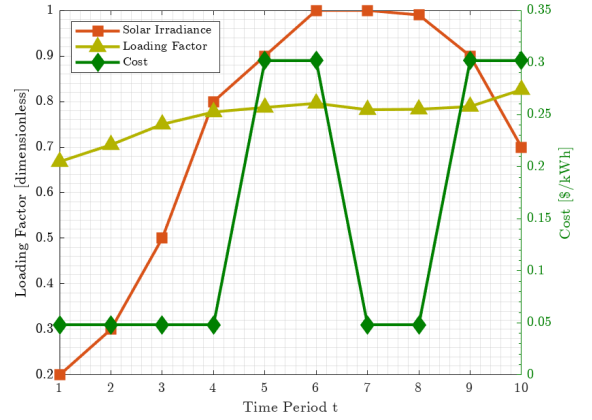


Fig. 6: Forecasts for Demand Power, Irradiance and Cost of Substation Power over a 10 Hour Horizon

- [15] M. I. Alizadeh and F. Capitanescu, "A tractable linearization-based approximated solution methodology to stochastic multi-period ac security-constrained optimal power flow," *IEEE Trans. Power Syst.*, vol. 38, no. 6, pp. 5896–5908, 2023.
- [16] M. Usman and F. Capitanescu, "Three solution approaches to stochastic multi-period ac optimal power flow in active distribution systems," *IEEE Transactions on Sustainable Energy*, vol. 14, no. 1, pp. 178–192, 2023.
- [17] N. Nazir and M. Almassalkhi, "Receding-Horizon Optimization of Unbalanced Distribution Systems with Time-Scale Separation for Discrete and Continuous Control Devices," pp. 1–7, Jun. 2018.
- [18] N. Nazir, P. Racherla, and M. Almassalkhi, "Optimal multi-period dispatch of distributed energy resources in unbalanced distribution feeders," Jun. 2019.
- [19] N. Nazir and M. Almassalkhi, "Guaranteeing a Physically Realizable

- Battery Dispatch Without Charge-Discharge Complementarity Constraints," *IEEE Trans. Smart Grid*, vol. 14, no. 3, pp. 2473–2476, Sep. 2021.
- [20] M. Farivar and S. H. Low, "Branch flow model: Relaxations and convexification," *2012 IEEE 51st IEEE Conference on Decision and Control (CDC)*, pp. 3672–3679, Dec. 2012.
- [21] A. Agarwal and L. Pileggi, "Large Scale Multi-Period Optimal Power Flow With Energy Storage Systems Using Differential Dynamic Programming," pp. 1750–1759, Sep. 2021.
- [22] X. Qian and Y. Zhu, "Differential Dynamic Programming for Multistage Uncertain Optimal Control," pp. 88–92, Jul. 2014.

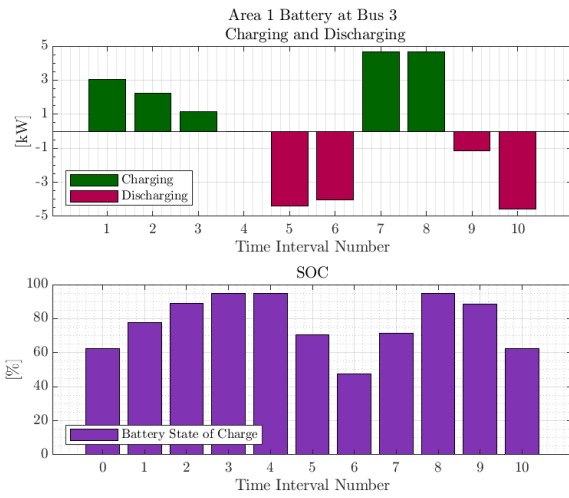


Fig. 7: Charging-Discharging and SOC graphs for Battery at Bus 3 located in Area 1 obtained via MPDOPF